https://doi.org/10.5194/egusphere-2026-4680
Preprint. Discussion started: 18 August 2026

Impact of Super Typhoon Yagi on Earth's Atmosphere: from Troposphere to Thermosphere/Ionosphere

Gang Chen[1]*, Peng Tao[1], Shaodong Zhang[1,2], Wanlin Gong[1], Chunming Huang[1], Yufang Tian[3], Yaxian Li[4,5], Kai Zhu[6], Xiaoming Zhou[1], Min Zhang[1], Yimeng Xu[1]

[1]School of Earth and Space Science and Technology, Wuhan University, Wuhan, 430000, China
[2]School of Physics and Electronic Science, Guizhou Normal University, Guiyang, 550000, China
[3]Key Laboratory of Middle Atmosphere and Global Environment Observation (LAGEO), Institute of Atmospheric Physics, Chinese Academy of Sciences, Beijing, 100000, China
[4]China Information Support Force Engineering University, Wuhan, 430000, China
[5]Suzhou Institute of Wuhan University, Suzhou, 215000, China
[6]School of Electronic Information, Wuhan University, Wuhan, 430000, China

Correspondence to: Gang Chen (g.chen@whu.edu.cn)

Abstract. Typhoons can generate gravity waves that transport energy and momentum from the lower atmosphere to the upper atmosphere, but the spectral characteristics and vertical coupling pathways of these disturbances remain incompletely understood. We investigate the atmospheric response to Super Typhoon Yagi (2024) by a Mesosphere-Stratosphere-Troposphere (MST) radar, two BeiDou Navigation Satellite System (BDS) receivers, and ERA5 reanalysis data. Great wind disturbances were observed in the troposphere and lower stratosphere by the MST radar, as Yagi passed approximately 188 km south of it. Gravity-wave activity was strongest between 5-12 km altitude and was dominated by periods of 0.6-5 h, with the maximum absolute momentum flux reaching 1.98 $m^2 s^{-2}$. ERA5 temperature perturbations revealed concentric wave structures centered near the typhoon eye, with amplitudes increasing from approximately 0.7 K at 20 km to more than 2 K at 50 km altitude. In mesosphere and lower thermosphere, enhanced and mutually consistent oscillations in the zonal, meridional, and vertical winds appeared on 7 Sept., with a dominant period near 2.0 h. Nearly simultaneous disturbances with a dominant period of approximately 2.1 h were detected in the total electron content of two BDS receivers. These observations provide evidence of typhoon-related disturbances extending from troposphere to thermosphere/ionosphere.

1 Introduction

Typhoons (tropical cyclones/hurricanes) are intense convective systems that not only cause catastrophic near-surface weather but also trigger complex dynamical processes from troposphere to upper atmosphere, establishing a key vertical coupling between the Earth's atmospheric layers (Dhaka et al., 2003; Pfister et al., 1993; Sato, 1993). Among these coupling mechanisms, Gravity waves (GWs) generated by typhoons are important carriers of energy and momentum, propagating upward to modulate the structure and dynamical characteristics of the stratosphere, mesosphere, thermosphere and ionosphere (Alexander et al., 1995; Chane Ming et al., 2010; Li et al., 2022). The propagation characteristics of the typhoon-produced GWs and the responses of the atmospheric layers to typhoons are crucial for understanding atmospheric coupling mechanisms and improving space weather forecasting.

Early observations based on Mesosphere-Stratosphere-Troposphere (MST) radars provided a fundamental understanding of typhoon-related GW activity. For example, Sato (1993) observed intense small-scale wind disturbances and inertial GWs in the lower stratosphere during the passage of Typhoon Kelly, revealing unique spectral characteristics and vertical propagation properties of the typhoon induced GWs. Dhaka et al. (2003) applied the MU radar to record the dominant GWs with periods of 7-8 minutes, 15 minutes, and 40-60 minutes in the upper troposphere and lower stratosphere during Typhoon 9426 (Orchid), and found that the wave amplitude decreased significantly after the typhoon passage. These radar-based observations confirm that typhoons are powerful sources of GWs, and wave generation is closely related to deep convection, topographic effects, and wind shear within the cyclonic system (Sato, 1993; Das et al., 2012).

Satellite observations have further expanded the global perspective of typhoon-induced GWs. Rakshit et al. (2018) used GPS radio occultation data from the Constellation Observing System for Meteorology, Ionosphere, and Climate (COSMIC) to show that the gravity wave potential energy in the lower stratosphere (19-26 km) increased along the typhoon track before the landfall of typhoons in the Bay of Bengal, with vertical wavelengths of 2-2.4 km carrying most of the wave energy. Chane Ming et al. (2010) analyzed GWs generated by intense tropical cyclones (e.g., Dina and Faxai) using GPS radiosonde profiles, emphasizing the correlation between wave characteristics and cyclone intensity and convective activity. In addition, combined satellite observations from instruments such as the Atmospheric Infrared Sounder (AIRS) and the Visible Infrared Imaging Radiometer Suite (VIIRS) have identified concentric GWs in the stratosphere and mesosphere over tropical cyclones, providing evidence for the upward propagation of GWs to mesospheric altitudes (Jana et al., 2020; Singh and Pallamraju, 2016; Xu et al., 2019). However, satellite observations generally lack the temporal resolution to capture rapid small-scale variations.

Numerical simulations have complemented observational results by investigating the generation mechanisms and propagation paths of the typhoon-induced GWs. Kim et al. (2005) conducted a numerical study on the GWs triggered by convection associated with Typhoon Rusa, emphasizing the role of deep convective upward motion in wave excitation. Pfister et al. (1993) simulated the GWs generated by tropical cyclone Jason using a three-dimensional transient linear gravity wave model, and the results showed that transient convective forcing with a spatial scale of ~100 km and a temporal scale of 4.5-6 hours could reproduce the wave characteristics observed in the lower stratosphere. Reanalysis data have also played a key role in validating these numerical results (Chane Ming et al., 2014; Kim et al., 2009; Fritts and Alexander, 2003; Wu et al., 2022).

Despite considerable progress in individual observational and numerical studies, there remain critical gaps in the comprehensive characterization of the cross-layer impacts of typhoons from troposphere to thermosphere/ionosphere. Most existing studies rely on single or limited observation platforms and lack the systematic integration of multi-instrument data, which hinders the holistic understanding of typhoon-induced cross-layer processes. In addition, the synergistic effect of the BeiDou Navigation Satellite System (BDS) ionospheric observations and multi-source atmospheric data in revealing the

https://doi.org/10.5194/egusphere-2026-4680
Preprint. Discussion started: 18 August 2026

vertical coupling chain has not been fully explored. Filling these gaps requires multi-instrument studies to capture the complete vertical range of typhoon impacts, which is essential for an in-depth understanding of cross-layer coupling processes and improving the predictive capability of typhoon-related atmospheric and ionospheric disturbances. MST radar is a powerful tool for atmospheric observation, and it can record the three-dimensional wind field variations in troposphere, stratosphere and mesosphere. Based on the observations of the MST radar located in Qinzhou, Guangxi, China, as well as other radio and optical observation systems, we introduce the impact of the super typhoon Yagi on the Earth's atmosphere.

2 Data and methods

2.1 Super Typhoon Yagi

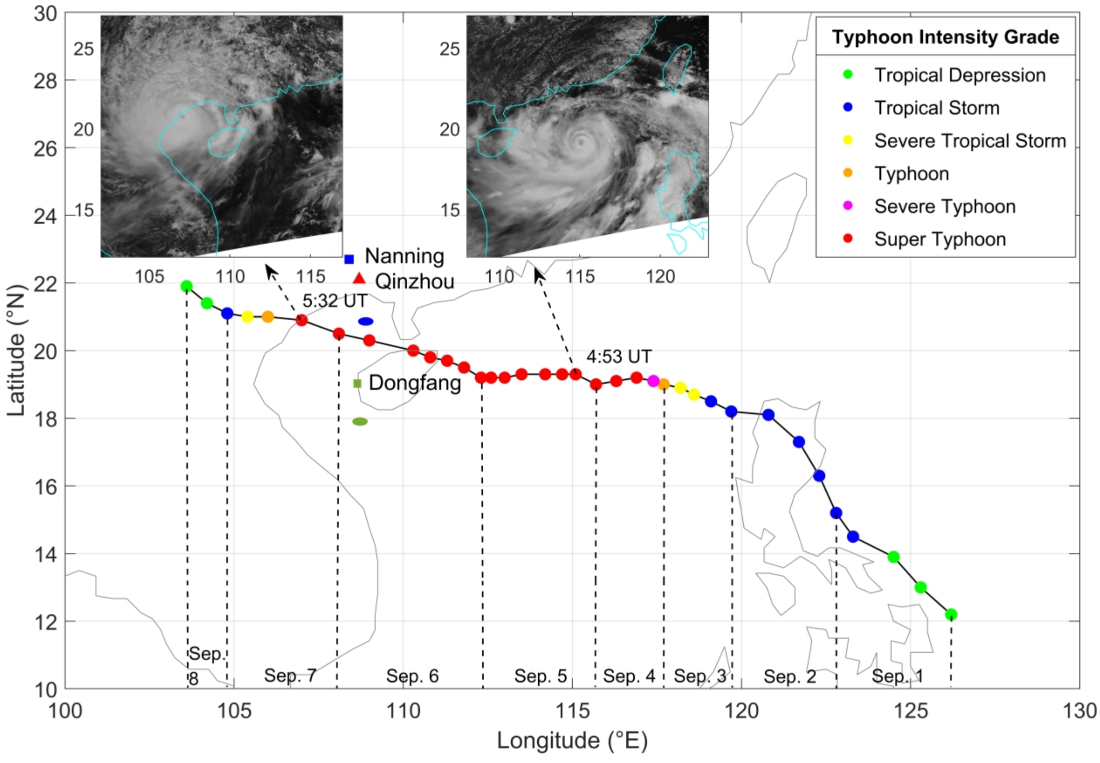

Figure 1. Map showing the path of Typhoon Yagi. The color of the dots on the typhoon path indicates typhoon intensity. The locations of the Chinese Low-latitude Atmosphere and Ionosphere Radar (CLAIR) in Qinzhou, two GNSS receivers in Nanning and Dongfang are shown as the red triangle and the blue and green squares, respectively. The corresponding puncture points of the satellite-ground link at 350 km altitude are indicated by the ellipses. Two snapshots of the typhoon at 04:53 UT on September 5 and 05:32 UT on September 7, 2024, are displayed at the top.

Yagi is the 11th typhoon in 2024, and its path is shown in the map of Fig. 1. Two snapshots of Yagi at 04:53 UT on September 5 and 05:32 UT on September 7 are shown at the top of Fig. 1. On September 1, Yagi formed over the sea east of the Philippines. It moved into the eastern South China Sea at 00:00 UT of September 3, and intensified to the severe tropical

https://doi.org/10.5194/egusphere-2026-4680
Preprint. Discussion started: 18 August 2026

storm level at 12:00 UT on September 3. Yagi has jumped three grades in intensity and evolved to super typhoon on September 4 (intensified to typhoon level at 00:00 UT, severe typhoon level at 06:00 UT, and super typhoon level at 15:00 UT). The maximum wind near the center increased to above level 17 at 15:00 UT on September 5 and maintained this level until it made landfall on the coastal area of Wengtian, Wenchang, Hainan around 08:20 UT on September 6 (above level 17, 62 m/s, minimum central pressure 915 hPa). After landfall, it passed through Haikou and moved into the Qiongzhou, then made a second landfall on Jiaowei, Xuwen, Guangdong around 14:20 UT on September 6 (level 17, 58 m/s), and subsequently moved into the Beibu Gulf. It made a third landfall on the southern coast of Quang Ninh, Vietnam around 07:30 UT on September 7 (level 17, 58 m/s). After landing in Vietnam, its intensity weakened rapidly, and it weakened to tropical storm at 21:00 UT on September 7, then dissipated. This study used the tropical cyclone best-track data from the China Meteorological Administration (Ying et al., 2014; Lu et al., 2021).

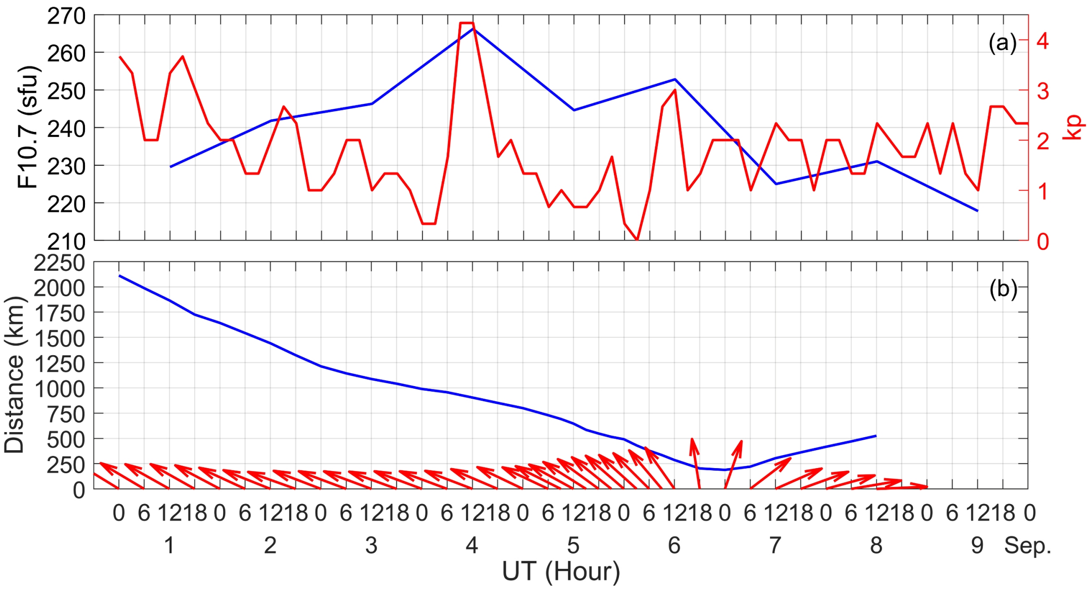

Figure 2. (a) F10.7 index (blue curve) and Kp index (red curve). (b) distance between the typhoon eye and the CLAIR (blue curve), and the direction of the typhoon eye to the radar (red arrow).

Figure 2a shows the Kp index (planetary K-index) (red curve) and F10.7 index (blue curve) from September 1 to 9, 2024. Kp index is used to characterize the magnitude of geomagnetic storms. During most time of those 9 days, Kp index was less than 3. On September 1, it reached 3.667 twice, and on September 4, it reached 4.333, indicating that the geomagnetic field is in an 'active' state, but has not yet reached the level of a geomagnetic storm. The solar radio flux at 10.7 cm (2800 MHz) is an excellent indicator of solar activity, and it is often called the F10.7 index. The F10.7 index in Fig. 2a indicates very high solar activity. It continued to rise from 229.5 sfu at 12:00 UT, Sep. 1, 2024. Until 12:00 UT on September 4, it reached a peak of 266.2 sfu and then started to decrease. At 12:00 UT on September 9, this index dropped to 217.8 sfu.

The MST radar located in Qinzhou, Guangxi, China (22.11° N, 108.66° E) is the main equipment for typhoon observation, and we also call it the Chinese Low-latitude Atmosphere and Ionosphere Radar (CLAIR). The blue curve in Fig. 2b shows

https://doi.org/10.5194/egusphere-2026-4680
Preprint. Discussion started: 18 August 2026

the temporal variation of the distance between the typhoon eye and the CLAIR. The typhoon approached the radar from the east, reaching its closest point to the radar at 21:00 UT on September 6, located 188 km south of the radar, and then moved westward away from the radar. The red arrows show the direction of the typhoon eye to the radar. Before approximately 21:00 UT on September 6, the typhoon was located southeast of the radar, after that, it was located southwest of the radar.

2.2 Qinzhou MST Radar/ CLAIR

Supported by the Meridian Project II of China, the CLAIR was completed construction in March 2024 and located in Qinzhou, Guangxi, China (22.11° N, 108.66° E) (Wang, 2010; Zhang et al., 2024) as indicated by the red triangle in Fig. 1. Two independent radar systems make up the CLAIR: one is a typical MST radar operated at 50 MHz frequency (CLAIR A) and the other is a dual-frequency radar working at 160 and 200 MHz frequencies (CLAIR B). The observation of the typhoon influence was implemented by the CLAIR A. It was operated in ST mode and M mode in turn. The radar formed five beams, one vertical beam and four oblique beams, to detect the echo Doppler velocities from five direction. Three-dimensional wind velocities, including zonal, meridional and vertical wind velocities, are estimated through the recorded Doppler velocities (Chinese Meridian Project, 2023). The eastward, northward and upward wind velocities are positive. The sampling period of wind velocity at each height bin is 15 minutes. The height resolutions below 25 km and above 60 km were 600 m and 1200 m, respectively. The maximum detectable wind speed is 234.38 m/s at troposphere and stratosphere height, and 146.48 m/s at mesosphere height.

2.3 ERA5

ERA5 is the fifth-generation atmospheric reanalysis dataset produced by the European Centre for Medium-Range Weather Forecasts (ECMWF). It provides hourly products covering atmospheric, ocean wave, and land surface variables. ERA5 is generated based on the four-dimensional variational data assimilation algorithm of the Integrated Forecast System (IFS), with a horizontal resolution of 0.25°×0.25°. Its atmospheric products contain 137 vertical pressure levels ranging from 1000 hPa to 0.01 hPa (Hersbach et al., 2020). ERA5 data are available for download from the Climate Data Store (https://cds.climate.copernicus.eu/datasets). The hourly atmospheric temperature data from ERA5 are adopted to investigated the influence of the typhoon.

2.4 VIIRS-DNB

The National Oceanic and Atmospheric Administration (NOAA) and the National Aeronautics and Space Administration (NASA) launched the Suomi National Polar-Orbiting Partnership (SNPP) satellite in 2011, followed by JPSS-1 in 2017 and JPSS-2 in 2022. All the three satellites are equipped with VIIRS. As a scanning optical sensor, the VIIRS achieves a spatial resolution of 0.724 km×0.724 km with a swath width of 3000 km, comprising 22 independent spectral bands (Miller et al., 2012). Among them, the Day/Night Band (DNB) has a spectral response range of 505-890 nm and a full spatial resolution of

https://doi.org/10.5194/egusphere-2026-4680
Preprint. Discussion started: 18 August 2026

750 m. Its sensitivity is approximately 106 times higher than that of conventional visible-light sensors, enabling detection of faint signals reflected from the ground and the Moon.

The VIIRS data are accessible from the NOAA Comprehensive Large Array-data Stewardship System (CLASS), which were used in the insets of Fig. 1 to show snapshots of the typhoon.

2.5 GNSS Ionospheric Monitor

BDS is a globally independent satellite navigation system developed by China. Unlike other Global Navigation Satellite Systems (GNSS), the BDS is equipped with five Geostationary Earth Orbit (GEO) satellites named C01-C05. The Ionospheric Pierce Point (IPP) of the BDS-GEO satellites remains stationary relative to ground stations, enabling continuous fixed-point monitoring of ionospheric total electron content (TEC), which offers unique advantage for ionosphere observation (Hu et al., 2017).

The ionospheric TEC and scintillation monitoring network of the Chinese Meridian Project consists of 32 stations that can receive signals from multiple GNSS constellations including the BDS and GPS, and their data are accessible via the official website of the Chinese Meridian Project. The vertical TEC (VTEC) data with a sampling rate of 1 Hz from the Nanning and Dongfang station are utilized to investigate the influence of the typhoon on ionosphere. The pierce points at 350 km altitude between the C03 satellite and the Nanning/Dongfang station are close to the CLAIR, as indicated by the blue/green ellipse in the map of Fig. 1. The blue IPP (108.7° E, 21.1° N) and the green IPP (108.8° E,17.9° N) are located on the north and south of the path of the typhoon, respectively.

https://doi.org/10.5194/egusphere-2026-4680
Preprint. Discussion started: 18 August 2026

3 Results and Analysis

3.1 Disturbances in Troposphere and Stratosphere

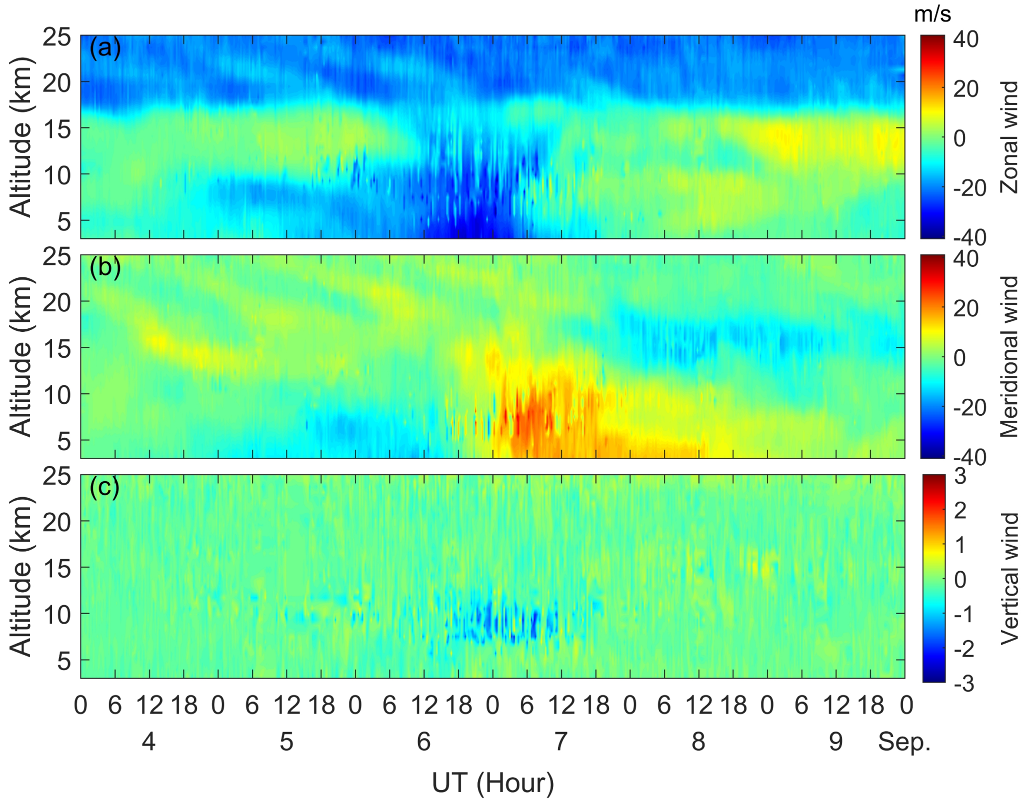

Figure 3. Variations of the tropospheric and low stratospheric wind fields observed by the CLAIR from September 4 to September 9. (a) Zonal wind, (b) meridional wind and (c) vertical wind variations are listed from top to bottom rows.

Typhoon Yagi passed slightly south of the CLAIR from east to west, with the closest distance of only about 188 km at 21:00 UT on September 6. Figure 3 shows the observational results of the three-dimensional wind field in the troposphere and lower stratosphere by the CLAIR in ST mode (15 min temporal resolution, 600 m altitude resolution) from September 4 to September 9, and sliding-window denoising was applied to the data beforehand. In Fig. 3a, the westward winds in the troposphere below 10 km altitude started to increase at 21:00 UT of September 4. The westward wind speed reached its maximum at approximately 21:00 UT on September 6, and the zonal winds recovered after 18:00 UT on September 7. The counterclockwise-rotating typhoon strengthened the westward winds in its northern part, and directly affected the stratosphere. From 18:00 UT on September 5, the westward wind field in the stratosphere descended from 17.7 km altitude, arrived 14.1 km altitude at 10:30 UT and connected with the westward wind field in the troposphere. At 01:45 UT on September 7, this connection disconnected. It indicates the occurrence of the stratosphere intrusion into the troposphere (Wang et al., 2025).

https://doi.org/10.5194/egusphere-2026-4680
Preprint. Discussion started: 18 August 2026

In Fig. 3b, the southward winds below 5 km altitude began to increase at 06:00 UT of September 5 When the Typhoon passed by, the southward winds turned to northward. Between 03:00-08:00 UT on September 7, the meridional wind disturbance has exceeded 15 km altitude. Obviously, while to the east and west of the radar, the typhoon strengthened southward and northward winds, respectively. Compared to the zonal winds, the impact of the Typhoon on the meridional winds appeared a little later, and finished much later. The meridional winds didn't recover until 03:00 UT on September 9. In Fig. 3c, there were evident disturbances in the vertical winds between 7-12.5 km altitude from 00:00 UT on September 6 to 00:00 UT on September 8. And these disturbances were mainly characterized by enhanced downward winds.

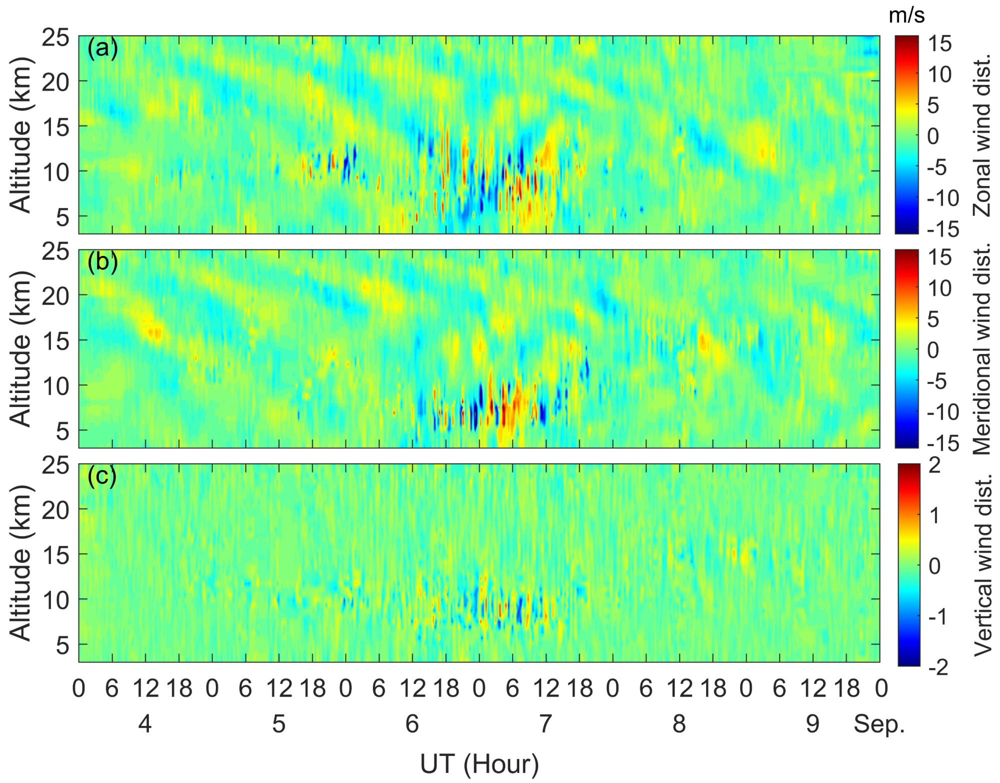

Figure 4. Total disturbances in (a) zonal wind, (b) meridional wind and (c) vertical wind variations with periods ranging from 0.6 to 31 hours.

To present the overall perturbation before and after the typhoon passage, a Butterworth filter was used to perform band-pass filtering on the above wind fields to obtain gravity wave perturbations within a period of 0.6-31 h (The calculated inertial period in the Qinzhou area is about 31 hours.). The results are shown in Fig. 4. There were a large number of high-frequency GWs excited at an altitude of about 5-14 km in the troposphere during the passage of the typhoon over the MST radar station, and they appeared mainly on September 6 and September 7.

The symmetric beam method proposed by Vincent et al. (Vincent, 1983) was applied to estimate the variations of the gravity wave momentum flux before and after the typhoon passage. In this method, the vertical flux of zonal (meridional) momentum is estimated by the following formulas:

https://doi.org/10.5194/egusphere-2026-4680
Preprint. Discussion started: 18 August 2026

$$MF_x = \frac{\overline{v_E'^2} - \overline{v_W'^2}}{2\sin 2\theta} \tag{1}$$

$$MF_y = \frac{\overline{v_N'^2} - \overline{v_S'^2}}{2\sin 2\theta} \tag{2}$$

where v_E'、v_w'、v_N'、v_S' are the radial wind perturbations in the east, west, north, and south directions, respectively, and θ is the zenith angle. Thus, the radial velocities recorded by the four oblique beams of the CLAIR are used to estimate the corresponding parameters. The four oblique beams point to due east, west, north, and south with 15° zenith angle. The absolute momentum flux is also estimated by the following formula:

$$AMF = \sqrt{MF_x^2 + MF_y^2} \tag{3}$$

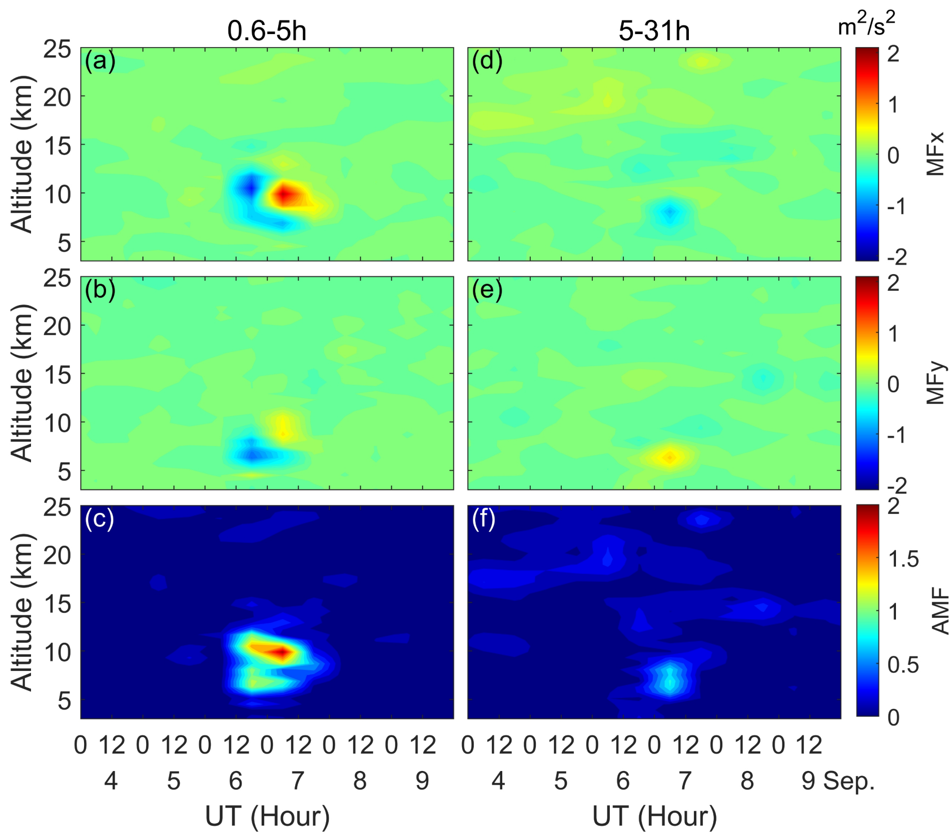

Figure 5. The 12-hour averaged zonal momentum flux (top row), meridional momentum flux (middle row), and absolute momentum flux (bottom row), which were calculated using the radial velocity data, with period ranges of 0.6-5 h and 5-31 h on the left and right sides, respectively.

To analyze the typhoon-excited GWs in different period bands, a Butterworth filter was applied to extract the wave perturbations within periods of 0.6-5 h and 5-31 h, respectively, Then, the 12-hour averaged momentum flux results are shown in Fig. 5. Evidently, between 12:00 UT on September 6 and 12:00 UT on September 7, the momentum flux of GWs

https://doi.org/10.5194/egusphere-2026-4680
Preprint. Discussion started: 18 August 2026

with periods of 0.6-5 h exhibited a significant enhancement. Specifically, the zonal momentum flux was mainly enhanced westward at 6-8 km, showed a westward-then-eastward variation at 8-12 km, and decreased rapidly above 12 km. The meridional momentum flux was enhanced southward at 5-8 km, mainly enhanced northward at 8-11 km, and decreased rapidly above 11 km. The maximum absolute momentum flux reached 1.98 $m^2\ s^{-2}$. During a similar time period, the momentum flux of GWs with periods of 5-31 h also showed an enhancement at approximately 5-8 km, but to a relatively lesser extent. This indicates that the GWs excited by the typhoon were dominated by short periods of 0.6-5 h.

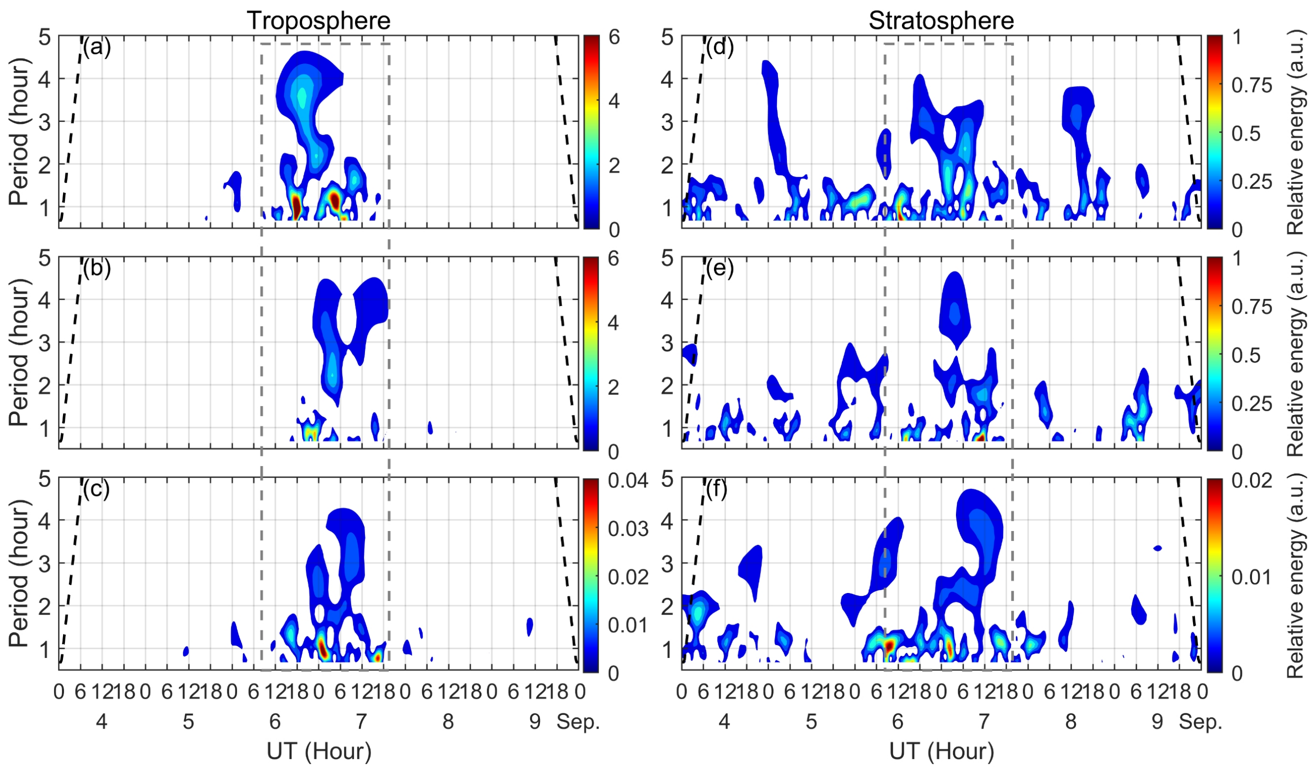

Figure 6. Averaged periodic waves in troposphere (left column) and stratosphere (right column). The waves in zonal winds, meridional winds and vertical winds are displayed in the top, middle and bottom rows, respectively. The black oblique lines represent the Cone of Influence (COI). The COI is defined as the region of the wavelet spectrum where edge effects become important (beginning and end of the data series). The typhoon related waves are highlighted by the gray boxes.

Based on the wave momentum fluxes in Fig. 5, the analytic Morlet wavelet analysis of the three-dimensional wind disturbances with periods of 0.6-5 h, averaged over the tropospheric and stratospheric height profiles, is shown in Fig. 6. To avoid potential contamination from the sharp background wind shear near the tropopause at approximately 17 km, the averaging was performed over the altitude ranges of 3-16 km and 18-25 km, respectively. The disturbances were extracted by removing the 25-point running-mean background and then applying a 0.6-5 h band-pass filter. As indicated by the gray box in the left column of Fig. 6, while the typhoon was passing the radar from 08:00 UT on September 6 to 19:00 UT on September 7, significant waves with periods of 0.6-4.5 h emerged. The period spectral in stratosphere in the right column of Fig. 6 are more complex, and there are many wave components appearing from September 4 to 9. But in the gray box, the

https://doi.org/10.5194/egusphere-2026-4680
Preprint. Discussion started: 18 August 2026

zonal, meridional and vertical winds all present the waves of 0.6-4.5 h period between 08:00 UT on September 6 and 19:00 UT on September 7, similar to that presented in the troposphere. In addition, the overall intensity of the stratospheric wave disturbances was relatively weaker. The specific reasons for this will be discussed in Sect. 4.

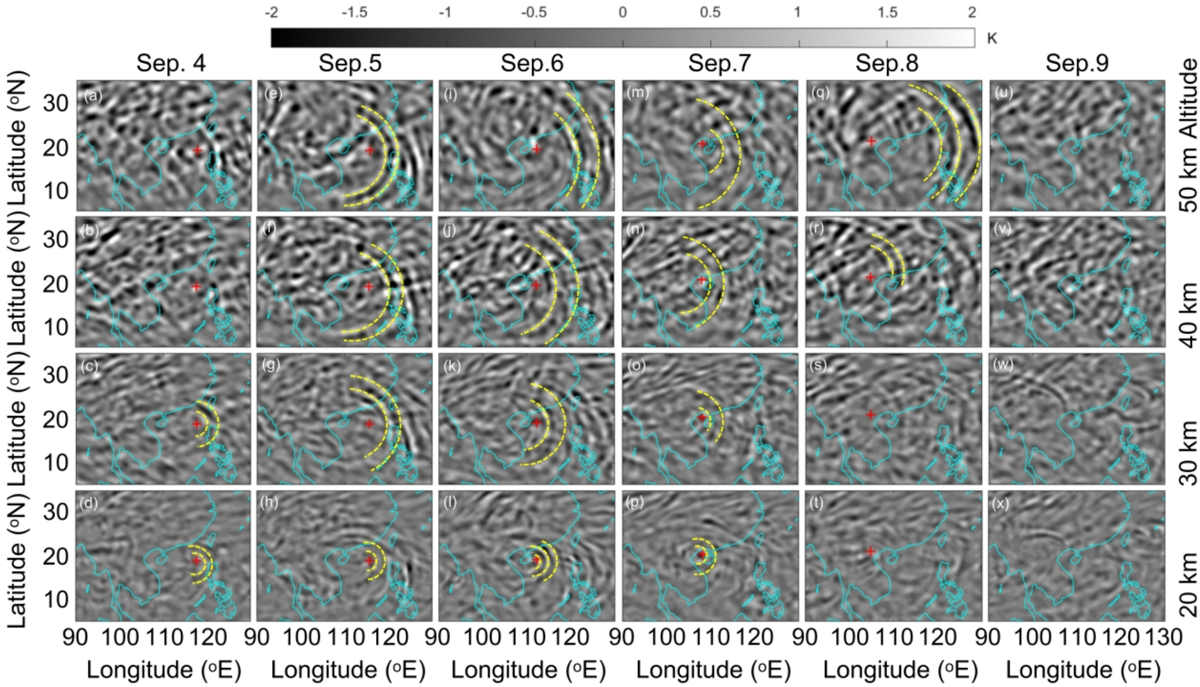

Figure 7. Temperature perturbations extracted from ERA5 data. The perturbations recorded at 00:00 UT each day from September 4 to 9 are listed from left to right column. The perturbations at 20, 30, 40, and 50 km altitude are displayed from bottom to top row. The red cross shows the location of the typhoon eye, and the yellow dashed curve indicates the wavefront.

At altitudes of 25-65 km in high stratosphere and low mesosphere, an MST radar usually can't effectively receive anything echoes, thus we examine the ERA5 reanalysis temperature data to investigate the typhoon related waves in this height range. Perturbations were extracted by subtracting the spatial background value of the surrounding 11×11 grid from the data at each pressure level, and then subtracting a 7-point moving average from the profile of each time. Figure 7 shows the results of regional perturbations at 00:00 UT daily from September 4 to 9 at altitudes of 20 km, 30 km, 40 km, and 50 km, respectively in stratosphere. The concentric GWs emerged in many subplots as indicated by the yellow dashed curves. The average perturbation intensity of the main concentric GWs at 20 km altitude was ~0.7 K in the bottom row of Fig. 7, and it increased with altitude, exceeding 2 K at 50 km altitude as shown in the top row of Fig. 7, and most of them propagated eastward. In addition, the centers of most of the recorded waves are almost located near the typhoon center as indicated by the red crosses.

3.2 Disturbances in Mesosphere and Lower Thermosphere

https://doi.org/10.5194/egusphere-2026-4680
Preprint. Discussion started: 18 August 2026

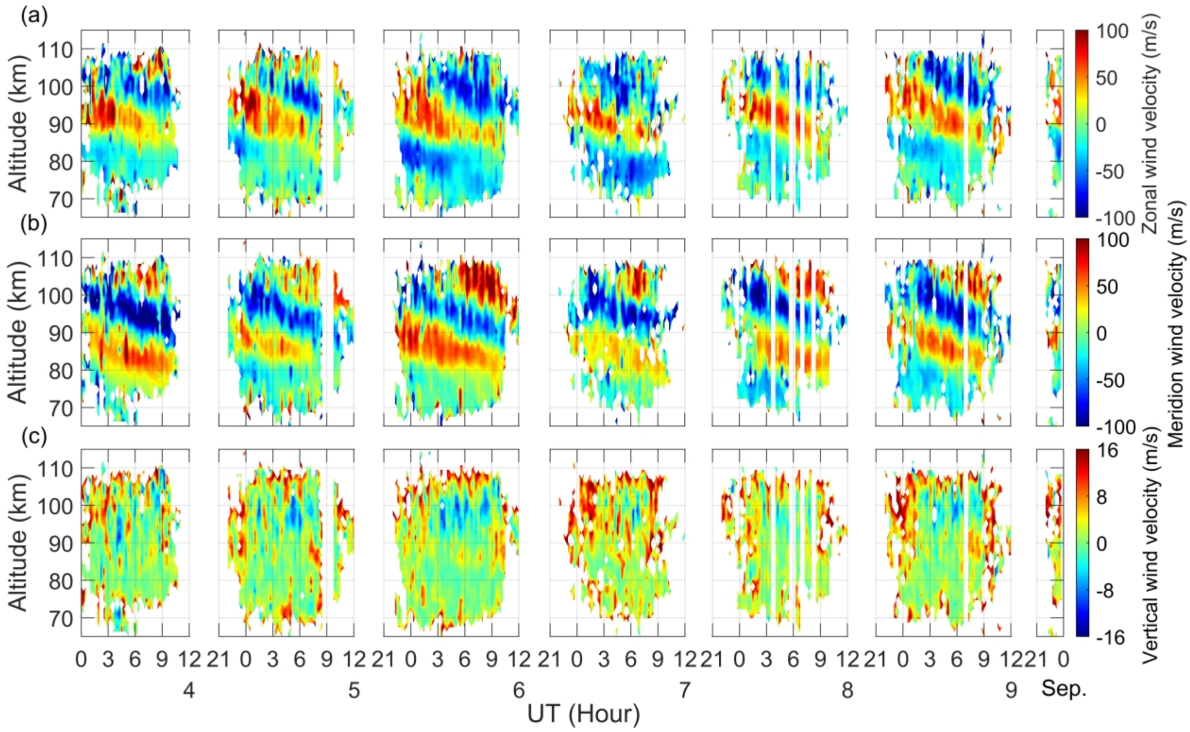

Figure 8. Wind field variations between 65 and 115 km altitude in mesosphere and low-thermosphere in the daytime from September 4 to 9. Zonal, meridional, and vertical wind field variations are displayed in top, middle and bottom rows, respectively. LT = UT + 8 h.

Figure 8 presents the three-dimensional wind field variations between 65-115 km altitudes observed by the CLAIR in M mode (15 min temporal resolution, 1.2 km altitude resolution), from which local nighttime periods and some invalid data with large deviations have been pre-removed. The echoes scattered from Mesosphere and Low Thermosphere (MLT) region usually occur in the daytime, thus we only present the data from 21:00-12:00 UT of the next day (5:00-20:00 LT) in each day. The zonal, meridional and vertical wind variations are presented in the top, middle and bottom row, respectively. The horizontal background wind fields are extremely strong, reaching several tens or even hundreds of meters per second, and exhibit obvious tidal pattern on each day, and there was no much disturbances emerged. The northward winds between 80-90 km altitude were smaller on September 7 than other days, and there were much stronger upward winds appearing at 80-100 km altitude on the same day.

https://doi.org/10.5194/egusphere-2026-4680
Preprint. Discussion started: 18 August 2026

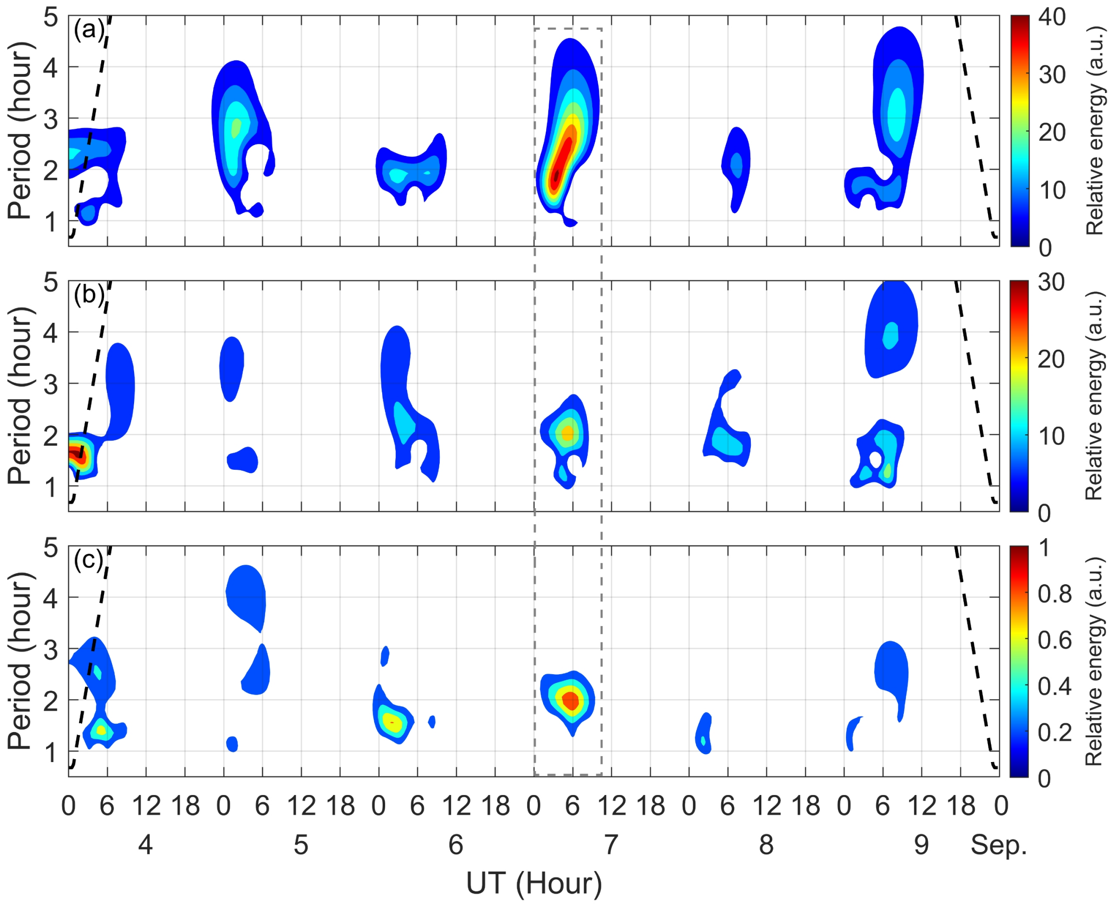

Figure 9. Periodic waves averaged over 75-100 km altitudes. The waves in zonal winds, meridional winds and vertical winds are displayed in the top, middle and bottom rows, respectively. The black oblique lines represent the COI. The typhoon related waves are highlighted by the gray box.

To facilitate the analysis of the propagation characteristics of typhoon-induced GWs in the MLT region, the following procedure was adopted to extract the mean wave disturbances in the MLT region. First, the data within the altitude range of 75-100 km and the time window of 00:00-09:30 UT per day were retained from Fig. 8, yielding six relatively complete data blocks. A sliding-window method was then applied to remove the strong background noise, and linear interpolation was used to replace the few data points outside the 00:00-09:30 UT daily window as well as all missing data. Subsequently, a three-point running mean was applied to further smooth the noise. Finally, a 0.6-5 h band-pass filter was applied to the data, followed by averaging along the altitude profile to obtain the three-dimensional wind disturbances averaged over the 75-100 km height range. The analytic Morlet wavelet analysis was then applied to these disturbances to obtain the time-period spectra in the MLT region, as shown in Fig. 9. The waves in the zonal, meridional and vertical winds are shown in the top, middle and bottom rows, respectively. It should be noted that although there are up to 14.5 hours of interpolation per day, the 0.6-5 h band-pass filter is sufficient to weaken its influence. During the daytime from September 4 to 9, some periodic

https://doi.org/10.5194/egusphere-2026-4680
Preprint. Discussion started: 18 August 2026

components appear in both the horizontal and vertical winds. But the periodic component on September 7 highlighted by the gray box was different from other days. The periodic waves on September 7 show higher intensity and a high level of consistency in the zonal, meridional, and vertical winds. The wave period is mainly concentrated between 1 to 3 hours and emerged from 0:00 to 10:00 UT, and exhibit nearly the same dominant period of approximately 2.0 hours across all three components. The range of the wave period in the MLT region is slightly smaller than that in the troposphere and stratosphere, especially the waves with periods of 0.5-1 h, which have almost disappeared.

3.3 Disturbances in Ionosphere

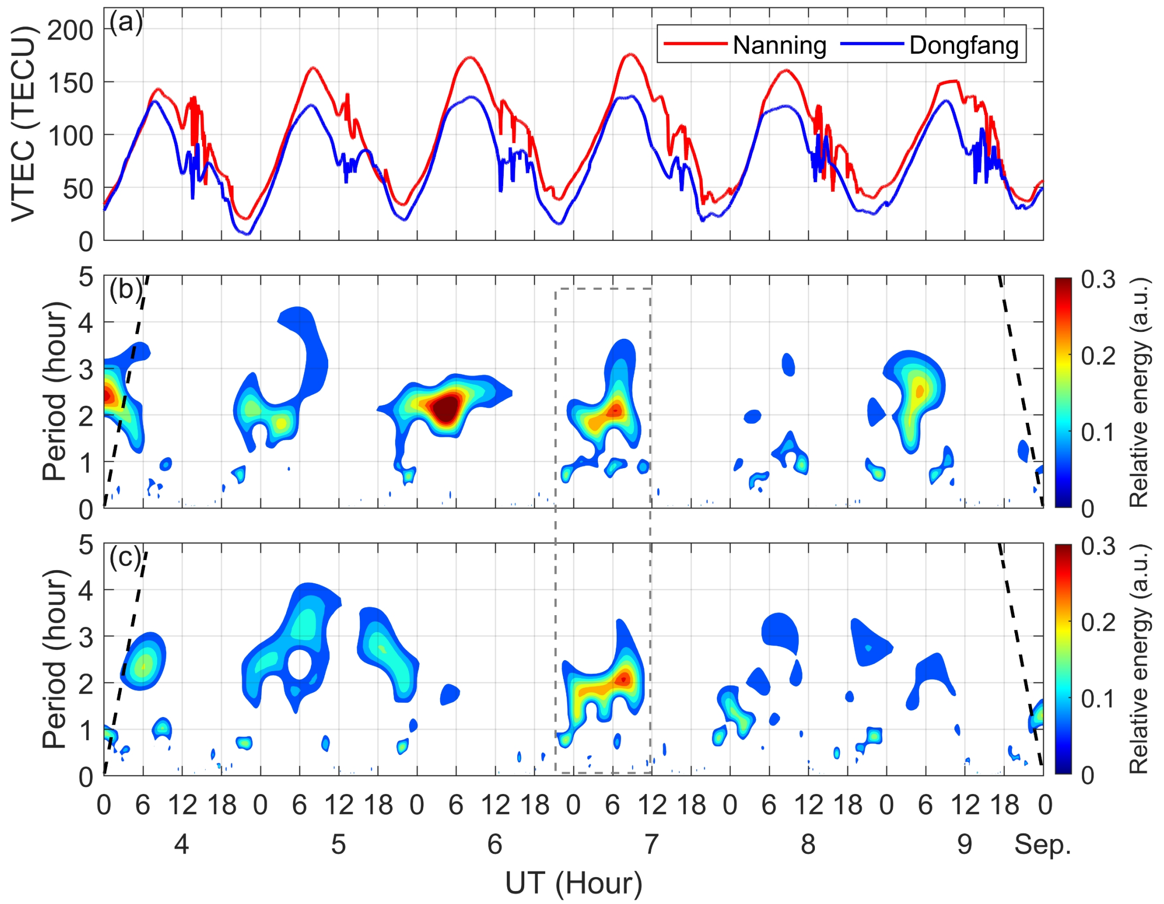

Figure 10. (a) Vertical TEC (VTEC) variation recorded by the GNSS receivers in Nanning (red curve) and Dongfang (blue curve). (b) and (c) Time-period spectrum of the red and blue TEC curves above, respectively. The black oblique lines represent the COI. The gray dashed box are used to highlight the possible typhoon induced waves. LT = UT + 8 h.

The VTEC variations recorded by the GNSS receivers in Nanning and Dongfang are shown in Fig. 10a by the red and blue curves. Please note that, since the raw data contain several jumps, for the convenience of spectral analysis, we pre-processed the data with jumps, and applied shape-preserving piecewise interpolation to fill the missing data. There are obvious

https://doi.org/10.5194/egusphere-2026-4680
Preprint. Discussion started: 18 August 2026

ionospheric day-to-day variations, and the nighttime ionosphere enhancements and equatorial plasma bubbles occurring after sunset (Zhang et al., 2026). To address this, a 5-hour window LOESS (LOcally Estimated Scatterplot Smoothing) method was applied to remove the background trend, followed by a 0.6-5 h band-pass filter to suppress high-frequency noise. Generally, ionospheric TEC disturbances induced by GWs are relatively small, typically not exceeding 1 TECU (Dube et al., 2020; Chen et al., 2020; Li et al., 2024). Therefore, we set all filtered data points with absolute values greater than 1 TECU to zero to minimize the influence of plasma bubbles. Finally, analytic Morlet wavelet analysis was applied to the residuals to obtain the time-period spectra of the VTEC disturbances at Nanning and Dongfang, as shown in Fig. 10b and 10c, respectively. Except for the waves in the gray dashed box, the wave periods recorded by the receivers in Nanning and Dongfang were totally different. But the periods within the gray dashed box exhibit a remarkable consistency, ranging from 0.6 to 3.6 hours between 22:00 UT on September 6 and 12:00 UT on September 7, and exhibited nearly the same dominant period of approximately 2.1 hours. This synchrony strongly suggests that these specific oscillations are not local phenomena but are instead driven by a common large-scale source, namely the passing typhoon.

4 Discussion

It is well known that MST radar has unique advantages in the field of atmospheric sounding, particularly excelling in observations of wind fields in the middle and upper atmosphere. Moreover, MST radar is capable of observing three-dimensional wind field variations, an advantage not shared by other instruments. As early as 1991, Sato et al. (1991) utilized the MU radar to conduct typhoon observations. However, despite the capability of MST radar to observe three-dimensional wind fields in the mesosphere, no observations to date have characterized mesospheric disturbances induced by typhoons based on MST radar measurements. This is likely because typhoons are often accompanied by severe winds, heavy rainfall, and lightning, which frequently force radio radar equipment to be shut down to avoid damage to antennas and instruments, thus missing the opportunity for close-range observation of the atmospheric effects of typhoons. During this super typhoon event, we maintained continuous operation under severe weather conditions and successfully obtained valuable data, especially three-dimensional wind field data in the MLT region.

As Typhoon Yagi passed over the CLAIR site from east to west, the CLAIR recorded significant wind field variations in the troposphere. The zonal wind exhibited a pronounced westward enhancement from 00:00 UT on 5 Sep. to 12:00 UT on 7 Sep., with a maximum exceeding 40 m/s. The meridional wind showed a southward intensification from 06:00 UT on 5 Sep. to 21:00 UT on 7 Sep., followed by a reversal and northward enhancement until 12:00 UT on 8 Sep.. The timing and orientation of these wind enhancements and reversals were highly correlated with the passage and location of Yagi. Furthermore, the prominent downward-sloping structures apparent in Fig. 3a likely indicate stratospheric intrusion processes. Indeed, troposphere-stratosphere exchange induced by tropical cyclones has been extensively studied (e.g., Leclair De Bellevue et al., 2006; Das, 2009; Das et al., 2016; Venkat Ratnam et al., 2016). This is not the focus of the present paper and will not be discussed in detail here.

The observational results demonstrate that Super Typhoon Yagi excited a broad spectrum of GWs in the troposphere, predominantly short-period GWs with periods of 0.6-5 hours, with gravity wave activity being particularly significant within the altitude range of 5-12 km. This altitude interval corresponds to the upper part of the typhoon's deep convective region and the lower part of the typhoon outflow layer, where strong latent heat release variations, vertical accelerations, and wind shears can effectively excite GWs. This wave source structure is consistent with previous radar, radiosonde, satellite, and numerical modeling studies, which have shown that tropical cyclones can excite GWs through convective heating, unbalanced motions near the vortex, and interactions between storm-scale circulations and environmental wind shears (Pfister et al., 1993; Sato, 1993; Dhaka et al., 2003; Kim et al., 2005; Chane Ming et al., 2010). Moreover, Kim et al. (2005) attributed the decrease in momentum flux with height in unfiltered regions to damping processes, which may similarly explain the rapid reduction in momentum flux observed above 13 km in our data.

Generally, rapidly evolving convective cells, the eyewall, and spiral rainband structures are more likely to excite relatively small-scale GWs, whereas storm-scale evolution and vortex adjustment processes may excite longer-period wave components (Pfister et al., 1993; Chane Ming et al., 2010; Kim et al., 2014). Therefore, the significant enhancement of gravity wave momentum flux in the 0.6-5 h period range likely reflects the direct forcing of GWs by intense convective activity within Yagi. Similar enhancements of short-period wave fluctuations were also reported in MU radar observations during the passages of Typhoon Kelly and Typhoon Orchid, where wind disturbances in the lower stratosphere were attributed to typhoon-excited GWs (Sato, 1993; Dhaka et al., 2003).

Concurrently, the tropospheric wind spectrograms show prominent fluctuations concentrated between 0.6-4.5 hours, spanning the period from 08:00 UT on 6 Sep. to 19:00 UT on 7 Sep., with highly consistent signatures across the three wind components. The mean spectrograms averaged over the 18-25 km altitude range in the stratosphere exhibit nearly identical spectral components during the same time period, but with relatively reduced intensity. Additionally, some fluctuations unrelated to the typhoon appear at other times, which may be attributable to gravity wave dissipation due to critical-level filtering (Cowling et al., 1971; Yue et al., 2009; Azeem et al., 2015; Singh and Pallamraju, 2016), resulting in substantial attenuation of the total gravity wave energy entering the stratosphere, such that the wave amplitudes no longer overwhelmingly dominate over non-typhoon-related fluctuations.

ERA5 temperature perturbations further reveal concentric gravity wave structures centered near the typhoon eye in the stratosphere. Such concentric wave patterns are typically associated with localized and transient wave sources, particularly deep convective activity embedded within tropical cyclones (Yue et al., 2013; Hoffmann et al., 2018; Wang et al., 2024). The perturbation amplitudes increase with height from 20 km to 50 km, consistent with the theoretical expectation of amplitude growth due to decreasing atmospheric density, provided that wave dissipation and critical-level absorption have not yet become dominant. However, this amplitude growth should not be simply interpreted as purely conservative propagation. Reanalysis data may smooth small-scale GWs, and the resolved perturbations likely represent only the larger-scale portion of the storm-excited wave spectrum. Thus, the ERA5 results are more suitable as evidence for large-scale

https://doi.org/10.5194/egusphere-2026-4680
Preprint. Discussion started: 18 August 2026

stratospheric gravity wave components excited by Yagi, whereas MST radar more effectively captures small-scale and high-frequency wave components near the source.

In the MLT region, the spectral analysis averaged over 75-100 km in Fig. 9 shows strong wave disturbances in all three wind components on 7 Sep., with a nearly consistent dominant period of 2.0 h, thereby indicating the propagation of a prevailing wave. Spectral analyses in the troposphere and stratosphere indicate that wave disturbances were strongly concentrated between 08:00 UT on 6 Sep. and 19:00 UT on 7 Sep.. Typically, the upward propagation time of convectively excited GWs to MLT altitudes ranges from tens of minutes to several hours, depending on the vertical group velocity of the waves, with higher-frequency waves exhibiting smaller propagation angles (Fritts and Alexander, 2003; Yue et al., 2013). The strongest period of wind disturbances in the MLT region would most likely occur on 7 Sep., and the results shown in Fig. 9 corroborate this expectation. Since MST radar observations of the MLT atmosphere are primarily conducted during daytime, the effective period for the spectral analysis shown in Fig. 9 should be between 00:00-09:00 UT each day; in fact, the disturbance duration is likely longer.

In ionosphere, the time-period diagrams in Fig. 10b and 10c show that both the Nanning and Dongfang stations exhibited strong TEC disturbances with a dominant period of approximately 2.1 h during nearly the same time window of 00:00-10:00 UT on 7 Sep., which is in excellent agreement with the 2.0 h prevailing wave observed in the MLT region in Fig. 9, both temporally and spatially strongly pointing to the underlying deep convective source associated with the typhoon. Indeed, the physical pathway from typhoon forcing to TEC disturbances is plausible. Through ion-neutral collisional coupling, GWs can induce plasma redistribution, resulting in quasi-periodic fluctuations in plasma density when observed at a fixed altitude (Azeem et al., 2015). At low latitudes, this coupling may also be amplified or modulated by electrodynamic processes, including the E-region dynamo, equatorial plasma instabilities, and magnetic-field-line-integrated plasma transport (Chou et al., 2017; Ajith et al., 2020; Jia et al., 2025). Previous studies have shown that tropical cyclones can excite concentric or asymmetric traveling ionospheric disturbances, and GWs may also seed or modulate equatorial plasma bubbles (Chou et al., 2017; Ajith et al., 2020; Dube et al., 2020; Fu and Jin, 2023).

A key question in typhoon-induced vertical coupling processes is which spectral components can continue to propagate upward. Figure 5 shows that short-period gravity wave momentum fluxes weaken significantly above approximately 13 km. Meanwhile, Fig. 3a shows strong westward background winds in the stratosphere, ERA5 results reveal eastward-propagating wave features in the stratosphere, and the spectral analysis also indicates that the mean spectral intensity averaged over 18-25 km in the stratosphere is markedly lower than that in the troposphere. These observations are consistent with background wind filtering and critical-layer processes: when the intrinsic frequency of a wave approaches zero, the wave encounters a critical layer and undergoes absorption or substantial attenuation (Fritts and Alexander, 2003; Liu and Meriwether, 2004). Similar filtering effects have been emphasized in multiple studies on GWs excited by typhoons and deep convection (Hoffmann et al., 2018; Kim et al., 2009; Wang et al., 2021). Furthermore, the wave periods observed in the MLT region and ionosphere are centered around 2 h, significantly narrower than the 0.6-4.5 h period range in the troposphere and lower stratosphere, further reflecting the selective role of the propagation environment. Figures 8a and 8b show strong tidal

https://doi.org/10.5194/egusphere-2026-4680
Preprint. Discussion started: 18 August 2026

signatures in the MLT region, which may further modulate GWs. GWs in the upper atmosphere are also prone to breaking upon reaching nonlinear saturation due to amplitude growth (Wang et al., 2023). The pronounced upward enhancement of vertical wind on 7 Sep. shown in Fig. 8c likely indicates the occurrence of gravity wave breaking. Fritts and Alexander (2003) noted that deviations from conservative propagation lead to energy dissipation and localized atmospheric heating. When a large number of GWs break in the MLT region and transfer heat to the background atmosphere, they can drive an upward enhancement of vertical wind. Therefore, the Yagi case demonstrates that vertical coupling efficiency is jointly controlled by typhoon forcing and the background atmospheric state, and the GWs with a dominant period of 2 h that ultimately reach ionospheric heights are likely the result of progressive filtering by the propagation environment.

5 Conclusions

We leveraged the high spatiotemporal resolution capability of the CLAIR for three-dimensional wind field observations in the troposphere, stratosphere, and mesosphere, together with ERA5 reanalysis and BDS observations, to investigate the atmospheric and ionospheric responses to Super Typhoon Yagi. Mainly based on the MST radar's ability to continuously observe three-dimensional wind fields at heights of 0-25 km and 75-110 km, we track the spectrum variations of the typhoon associated GWs from troposphere to thermosphere/ionosphere. It is a first investigation to use MST radar to investigate the propagation of typhoon-excited GWs from the lower atmosphere to the upper atmosphere, and it is also the first time to examine the vertical coupling characteristics from the lower atmosphere to the ionosphere induced by a typhoon through cross-sphere wave spectral analysis. These observations will deep our understanding of the vertical coupling efficiency controlled jointly by the typhoon forcing and the propagation environment for gravity waves.

Data availability

The data of the Qinhzou MST radar (CLAIR) and ionospheric TEC can be publicly obtained from https://dcstatus.meridianproject.ac.cn/#/sjfw/sjjs (Meridian Project Data Center, 2023). The ERA5 reanalysis data are available from the Copernicus Climate Change Service Climate Data Store at https://doi.org/10.24381/cds.bd0915c6 (Hersbach et al., 2023). VIIRS DNB data are available from the NOAA CLASS (https://www.aev.class.noaa.gov, Miller et al., 2012). The Kp and F10.7 indices (Matzka et al., 2021) are available from https://kp.gfz.de/en/data. The typhoon best-track data can be obtained from the China Meteorological Administration at https://tcdata.typhoon.org.cn (Ying et al., 2014; Lu et al., 2021).

Author contributions

GC conceived the idea of this manuscript. PT carried out the data analysis, interpretation, and manuscript preparation. GC investigated the physicochemical mechanisms and revised the manuscript. SZ, WG, CH, KZ, and XZ organized the datasets. YT, YL, MZ, and YX provided valuable suggestions. All authors discussed the results and commented on the manuscript.

Competing interests

The contact author has declared that none of the authors has any competing interests.

Acknowledgements

We acknowledge the use of data from the Chinese Meridian Project. We appreciate the China Meteorological Administration for the provision of typhoon best-track data. We thank the European Centre for Medium-Range Weather Forecasts (ECMWF) for the provision of the ERA5 data and the NOAA CLASS for providing DNB data.

Financial support

This research was supported by the National Natural Science Foundation of China (42274197) and the Basic Research Program of Jiangsu (Grant BK20250448).

References

Ajith, K. K., Li, G., Tulasi Ram, S., Yamamoto, M., Hozumi, K., Abadi, P., and Xie, H.: On the seeding of periodic equatorial plasma bubbles by gravity waves associated with tropical cyclone: A case study, J. Geophys. Res. Space Phys., 125, e2020JA028003, https://doi.org/10.1029/2020JA028003, 2020.

Alexander, M. J., Holton, J. R., and Durran, D. R.: The gravity wave response above deep convection in a squall line simulation, J. Atmos. Sci., 52(12), 2212-2226, https://doi.org/10.1175/1520-0469(1995)052%3C2212:TGWRAD%3E2.0.CO;2, 1995.

Azeem, I., Yue, J., Hoffmann, L., Miller, S. D., Straka, W. C., III, and Crowley, G.: Multisensor profiling of a concentric gravity wave event propagating from the troposphere to the ionosphere, Geophys. Res. Lett., 42(19), 7874-7880, https://doi.org/10.1002/2015GL065903, 2015.

Chane Ming, F., Chen, Z., and Roux, F.: Analysis of gravity-waves produced by intense tropical cyclones, Ann. Geophys., 28(2), 531-547, https://doi.org/10.5194/angeo-28-531-2010, 2010.

Chane Ming, F., Ibrahim, C., Barthe, C., Jolivet, S., Keckhut, P., Liou, Y. A., and Kuleshov, Y.: Observation and a numerical study of gravity waves during tropical cyclone Ivan (2008), Atmos. Chem. Phys., 14(2), 641-658, https://doi.org/10.5194/acp-14-641-2014, 2014.

Chen, J., Zhang, X., Ren, X., Zhang, J., Freeshah, M., and Zhao, Z.: Ionospheric disturbances detected during a typhoon based on GNSS phase observations: A case study for typhoon Mangkhut over Hong Kong, Adv. Space Res., 66(7), 1743-1753, https://doi.org/10.1016/j.asr.2020.06.006, 2020.

Chou, M. Y., Lin, C. C., Yue, J., Tsai, H. F., Sun, Y. Y., Liu, J. Y., and Chen, C. H.: Concentric traveling ionosphere disturbances triggered by Super Typhoon Meranti (2016), Geophys. Res. Lett., 44(3), 1219-1226, https://doi.org/10.1002/2016GL072205, 2017.

Cowling, D. H., Webb, H. D., and Yeh, K. C.: Group rays of internal gravity waves in a wind-stratified atmosphere, J. Geophys. Res., 76(1), 213-220, https://doi.org/10.1029/JA076i001p00213, 1971.

Das, S. S.: A new perspective on MST radar observations of stratospheric intrusions into troposphere associated with tropical cyclone, Geophys. Res. Lett., 36(15), https://doi.org/10.1029/2009GL039184, 2009.

Das, S. S., Uma, K. N., and Das, S. K.: MST radar observations of short-period gravity wave during overhead tropical cyclone, Radio Sci., 47(2), 1-10, https://doi.org/10.1029/2011RS004840, 2012.

Das, S. S., Venkat Ratnam, M., Uma, K. N., Patra, A. K., Subrahmanyam, K. V., Girach, I. A., and Ramkumar, G.: Stratospheric intrusion into the troposphere during the tropical cyclone Nilam (2012), Q. J. R. Meteorol. Soc., 142(698), 2168-2179, https://doi.org/10.1002/qj.2810, 2016.

Dhaka, S. K., Takahashi, M., Shibagaki, Y., Yamanaka, M. D., and Fukao, S.: Gravity wave generation in the lower stratosphere due to passage of the typhoon 9426 (Orchid) observed by the MU radar at Shigaraki (34.85° N, 136.10° E), J. Geophys. Res. Atmos., 108(D19), https://doi.org/10.1029/2003JD003489, 2003.

Dube, A., Singh, R., Maurya, A. K., Kumar, S., Sunil, P. S., and Singh, A. K.: Ionospheric perturbations induced by a very severe cyclonic storm (VSCS): A case study of Phailin VSCS, J. Geophys. Res. Space Phys., 125(1), e2019JA027197, https://doi.org/10.1029/2019JA027197, 2020.

Fritts, D. C., and Alexander, M. J.: Gravity wave dynamics and effects in the middle atmosphere, Rev. Geophys., 41(1), 1003, https://doi.org/10.1029/2001RG000106, 2003.

Fu, J., and Jin, S.: Characterization of ionospheric disturbances following multiple typhoons using GPS-derived TEC, J. Geophys. Res. Space Phys., 128(1), e2022JA030457, https://doi.org/10.1029/2022JA030457, 2023.

Hersbach, H., Bell, B., Berrisford, P., Hirahara, S., Horányi, A., Muñoz-Sabater, J., and Thépaut, J. N.: The ERA5 global reanalysis, Q. J. R. Meteorol. Soc., 146(730), 1999-2049, https://doi.org/10.1002/qj.3803, 2020.

Hersbach, H., Bell, B., Berrisford, P., Biavati, G., Horányi, A., Muñoz Sabater, J., Nicolas, J., Peubey, C., Radu, R., Rozum, I., Schepers, D., Simmons, A., Soci, C., Dee, D., and Thépaut, J.- N.: ERA5 hourly data on pressure levels from 1940 to present, Copernicus Climate Change Service (C3S) Climate Data Store (CDS) [data set], https://doi.org/10.24381/cds.bd0915c6, 2023.

Hoffmann, L., Wu, X., and Alexander, M. J.: Satellite observations of stratospheric gravity waves associated with the intensification of tropical cyclones, Geophys. Res. Lett., 45(3), 1692-1700, https://doi.org/10.1002/2017GL076123, 2018.

Hu, L., Yue, X., and Ning, B.: Development of the Beidou Ionospheric Observation Network in China for space weather monitoring, Space Weather, 15(8), 974-984, https://doi.org/10.1002/2017SW001636, 2017.

Jana, S., Rakshit, G., and Maitra, A.: Gravity wave activities associated with convective phenomena at a tropical location near land-sea boundary, Radio Sci., 55(1), 1-13, https://doi.org/10.1029/2019RS006952, 2020.

Jia, Y., Chen, G., Xu, J., Yan, C., Zhang, S., Hu, L., et al.: Why do small-scale irregularities migrate beyond the equatorial plasma bubble?, Geophys. Res. Lett., 52, e2024GL114399, https://doi.org/10.1029/2024GL114399, 2025.

Kim, S. Y., Chun, H. Y., and Baik, J. J.: A numerical study of gravity waves induced by convection associated with Typhoon Rusa, Geophys. Res. Lett., 32(24), https://doi.org/10.1029/2005GL024662, 2005.

Kim, S. Y., Chun, H. Y., and Wu, D. L.: A study on stratospheric gravity waves generated by Typhoon Ewiniar: Numerical simulations and satellite observations, J. Geophys. Res. Atmos., 114(D22), https://doi.org/10.1029/2009JD011971, 2009.

Kim, S. H., Chun, H. Y., and Jang, W.: Horizontal divergence of typhoon-generated gravity waves in the upper troposphere and lower stratosphere (UTLS) and its influence on typhoon evolution, Atmos. Chem. Phys., 14(7), 3175-3182, https://doi.org/10.5194/acp-14-3175-2014, 2014.

Leclair De Bellevue, J., Réchou, A., Baray, J. L., Ancellet, G., and Diab, R. D.: Signatures of stratosphere to troposphere transport near deep convective events in the southern subtropics, J. Geophys. Res. Atmos., 111(D24), https://doi.org/10.1029/2005JD006947, 2006.

Li, K., Zhang, D., Zeng, Y., Tian, Y., Dai, G., Liu, Z., et al.: Revisiting the ionospheric disturbances over low latitude region of China during super typhoon Hato, Space Weather, 22, e2023SW003694, https://doi.org/10.1029/2023SW003694, 2024.

Li, Q., Xu, J., Liu, H., Liu, X., and Yuan, W.: How do gravity waves triggered by a typhoon propagate from the troposphere to the upper atmosphere?, Atmos. Chem. Phys., 22(18), 12077-12091, https://doi.org/10.5194/acp-22-12077-2022, 2022.

Liu, H. L., and Meriwether, J. W.: Analysis of a temperature inversion event in the lower mesosphere, J. Geophys. Res. Atmos., 109(D2), https://doi.org/10.1029/2002JD003026, 2004.

Lu, X. Q., Yu, H., Ying, M., Zhao, B. K., Zhang, S., Lin, L. M., Bai, L. N., and Wan, R. J.: Western North Pacific tropical cyclone database created by the China Meteorological Administration, Adv. Atmos. Sci., 38(4), 690-699, https://doi.org/10.1007/s00376-020-0211-7, 2021 (data available at: https://tcdata.typhoon.org.cn, last access: 1 August 2026).

Matzka, J., Stolle, C., Yamazaki, Y., Bronkalla, O., and Morschhauser, A.: The geomagnetic Kp index and derived indices of geomagnetic activity, Space Weather, 19(5), e2020SW002641, https://doi.org/10.1029/2020SW002641, 2021 (data available at: https://kp.gfz.de/en/data, last access: 1 August 2026).

Meridian Project Data Center: MST radar and ionospheric TEC data [data set], https://dcstatus.meridianproject.ac.cn/#/sjfw/sjjs (last access: 1 August 2026), 2023.

Miller, S. D., Mills, S. P., Elvidge, C. D., Lindsey, D. T., Lee, T. F., and Hawkins, J. D.: Suomi satellite brings to light a unique frontier of nighttime environmental sensing capabilities, Proc. Natl. Acad. Sci. USA, 109(39), https://doi.org/10.1073/pnas.1207034109, 2012 (data available at: https://www.aev.class.noaa.gov, last access: 1 August 2026).

Pfister, L., Chan, K. R., Bui, T. P., Bowen, S., Legg, M., Gary, B., and Starr, W.: Gravity waves generated by a tropical cyclone during the STEP tropical field program: A case study, J. Geophys. Res. Atmos., 98(D5), 8611-8638, https://doi.org/10.1029/92JD01679, 1993.

Rakshit, G., Jana, S., and Maitra, A.: Gravity wave behavior in lower stratosphere during tropical cyclones over the Bay of Bengal, Radio Sci., 53(11), 1356-1367, https://doi.org/10.1029/2018RS006614, 2018.

Sato, K.: Small-scale wind disturbances observed by the MU radar during the passage of Typhoon Kelly, J. Atmos. Sci., 50(4), 518-537, https://doi.org/10.1175/1520-0469(1993)050%3C0518:SSWDOB%3E2.0.CO;2, 1993.

Sato, T., Ao, N., Yamamoto, M., Fukao, S., Tsuda, T., and Kato, S.: A typhoon observed with the MU radar, Mon. Weather Rev., 119(3), 755-768, https://doi.org/10.1175/1520-0493(1991)119%3C0755:ATOWTM%3E2.0.CO;2, 1991.

Singh, R. P., and Pallamraju, D.: Effect of cyclone Nilofar on mesospheric wave dynamics as inferred from optical nightglow observations from Mount Abu, India, J. Geophys. Res. Space Phys., 121(6), 5856-5867, https://doi.org/10.1002/2016JA022412, 2016.

Vadas, S. L., Fritts, D. C., and Alexander, M. J.: Mechanism for the generation of secondary waves in wave breaking regions, J. Atmos. Sci., 60(1), 194-214, https://doi.org/10.1175/1520-0469(2003)060%3C0194:MFTGOS%3E2.0.CO;2, 2003.

Venkat Ratnam, M., Ravindra Babu, S., Das, S. S., Basha, G., Krishnamurthy, B. V., and Venkateswararao, B.: Effect of tropical cyclones on the stratosphere-troposphere exchange observed using satellite observations over the north Indian Ocean, Atmos. Chem. Phys., 16(13), 8581-8591, https://doi.org/10.5194/acp-16-8581-2016, 2016.

Vincent, R. A., and Reid, I. M.: HF Doppler measurements of mesospheric gravity wave momentum fluxes, J. Atmos. Sci., 40(5), 1321-1333, https://doi.org/10.1175/1520-0469(1983)040%3C1321:HDMOMG%3E2.0.CO;2, 1983.

Wang, C.: New chains of space weather monitoring stations in China, Space Weather, 8, https://doi.org/10.1029/2010SW000603, 2010.

Wang, J., Chen, G., Zhang, S., Zhang, W., He, Z., Huang, K., and Huang, C.: Mid-latitude mesospheric responses of the solar eclipse on 21 June 2020 observed by the Wuhan MST radar, J. Geophys. Res. Space Phys., 128, e2022JA030892, https://doi.org/10.1029/2022JA030892, 2023.

Wang, X., Zhang, L., Wang, Y., and Zhang, Y.: Influences of the mid-latitude westerly trough on stratospheric gravity waves generated by Typhoon Lekima (2019), J. Geophys. Res. Atmos., 126(23), e2021JD035399, https://doi.org/10.1029/2021JD035399, 2021.

Wang, X., Wang, Y., Zhang, L., Zhang, Y., and Guan, J.: A climatology of stratospheric gravity waves induced by tropical cyclones on the northwest Pacific Ocean, npj Clim. Atmos. Sci., 7(1), 155, https://doi.org/10.1038/s41612-024-00705-2, 2024.

https://doi.org/10.5194/egusphere-2026-4680
Preprint. Discussion started: 18 August 2026

Wang, Y., He, Y., Tao, Y., Ren, Y., and Sheng, Z.: Super typhoon triggers severe ozone pollution in Pearl River Delta via stratospheric intrusion, Environ. Res. Lett., 20(12), 124082, https://doi.org/10.1088/1748-9326/ae23e7, 2025.

Wu, X., Hoffmann, L., Wright, C. J., Hindley, N. P., Kalisch, S., Alexander, M. J., and Wang, Y.: Stratospheric gravity waves as a proxy for hurricane intensification: A case study of weather research and forecast simulation for Hurricane Joaquin, Geophys. Res. Lett., 49(1), e2021GL097010, https://doi.org/10.1029/2021GL097010, 2022.

Xu, S., Yue, J., Xue, X., Vadas, S. L., Miller, S. D., Azeem, I., and Zhang, S.: Dynamical coupling between Hurricane Matthew and the middle to upper atmosphere via gravity waves, J. Geophys. Res. Space Phys., 124(5), 3589-3608, https://doi.org/10.1029/2018JA026453, 2019.

Ying, M., Zhang, W., Yu, H., Lu, X., Feng, J., Fan, Y., Zhu, Y., and Chen, D.: An overview of the China Meteorological Administration tropical cyclone database, J. Atmos. Oceanic Technol., 31, 287-301, https://doi.org/10.1175/JTECH-D-12-00119.1, 2014 (data available at: https://tcdata.typhoon.org.cn, last access: 1 August 2026).

Yue, J., Vadas, S. L., She, C.-Y., Nakamura, T., Reising, S. C., Liu, H.-L., Stamus, P., Krueger, D. A., Lyons, W., and Li, T.: Concentric gravity waves in the mesosphere generated by deep convective plumes in the lower atmosphere near Fort Collins, Colorado, J. Geophys. Res., 114, D06104, https://doi.org/10.1029/2008JD011244, 2009.

Yue, J., Hoffmann, L., and Alexander, M. J.: Simultaneous observations of convective gravity waves from a ground-based airglow imager and the AIRS satellite experiment, J. Geophys. Res. Atmos., 118(8), 3178-3191, https://doi.org/10.1002/jgrd.50341, 2013.

Zhang, M., Chen, G., Xu, J., Yan, C., Yang, M., Wu, K., et al.: Equatorial plasma bubbles encounter with the nighttime ionosphere enhancement, J. Geophys. Res. Space Phys., 131, e2024JA033324, https://doi.org/10.1029/2024JA033324, 2026.

Zhang, S., Chen, G., Gong, W., Liu, Y., Xiao, Q., Zhou, X., ... and Zhou, G.: Chinese Low-Latitude Atmosphere and Ionosphere Radar (CLAIR) of Meridian Project II: System description and initial observation results, IEEE Trans. Geosci. Remote Sens., 62, 1-9, https://doi.org/10.1109/TGRS.2024.3506774, 2024.